
iRNN: INTEGER-ONLY RECURRENT NEURAL NETWORK

A PREPRINT

Eyyüb Sari

Huawei Noah's Ark Lab
eyyub.sari@huawei.com

Vanessa Courville

Huawei Noah's Ark Lab
vanessa.courville@huawei.com

Vahid Partovi Nia

Huawei Noah's Ark Lab
vahid.partovinia@huawei.com

September 22, 2021

ABSTRACT

Recurrent neural networks (RNN) are used in many real-world text and speech applications. They include complex modules such as recurrence, exponential-based activation, gate interaction, un-foldable normalization, bi-directional dependence, and attention. The interaction between these elements prevents running them on integer-only operations without a significant performance drop. Deploying RNNs that include layer normalization and attention on integer-only arithmetic is still an open problem. We present a quantization-aware training method for obtaining a highly accurate integer-only recurrent neural network (iRNN). Our approach supports layer normalization, attention, and an adaptive piecewise linear approximation of activations, to serve a wide range of RNNs on various applications. The proposed method is proven to work on RNN-based language models and automatic speech recognition. Our iRNN maintains similar performance as its full-precision counterpart, their deployment on smartphones improves the runtime performance by $2\times$, and reduces the model size by $4\times$.

1 Introduction

RNN (Rumelhart et al., 1986) architectures such as LSTM Hochreiter and Schmidhuber (1997) or GRU Cho et al. (2014) are the backbones of many downstream applications. RNNs now are part of large-scale systems such as neural machine translation Chen et al. (2018); Wang et al. (2019a) and on-device systems such as Automatic Speech Recognition (ASR) He et al. (2019). RNNs are still highly used architectures in academia and industry, and their efficient inference requires more elaborated studies.

Recently, Transformer-based models (Vaswani et al., 2017; Devlin et al., 2019) have been proposed as an alternative to RNNs. Transformers enjoy from massively parallel training, which improves their ability to scale thank to this parallel implementation property. However, RNNs, specially LSTMs are still major tools in building highly accurate models in industry. The combination of LSTM and transformer have provided impressive results recently; Chen et al. (2018) and Wang et al. (2019a) proposed an encoder-decoder neural machine translator which harvests the inherent parallelism of transformers for the encoder while utilizing LSTMs for a faster decoder. In their study, the LSTM decoder achieved a faster inference runtime than a transformer decoder. The low performance of transformer models is due to losing their parallelization capabilities when generating outputs based on conditional inputs. Moreover, they still suffer from quadratic computation complexity with respect to the sequence length (Wang et al., 2019a). Kasai et al. (2021) took transformers one step further and finetuned a pretrained transformer into RNNs, benefiting the best of the two worlds.

In many edge devices, the number of computing cores is limited to a handful of computing units, in which parallel-friendly transformer-based models lose their advantage. There have been several studies in quantizing transformers to adapt them for edge devices but RNNs are largely ignored. Deploying RNN-based chatbot, conversational agent, and ASR on edge devices with limited memory and energy requires further computational improvements. The 8-bit integer neural networks quantization (Jacob et al., 2017) for convolutional architectures (CNNs) is shown to be an almost free lunch to tackle the memory, energy, and latency costs, with a negligible accuracy drop (Krishnamoorthi, 2018). Intuitively, quantizing RNNs is more challenging because the errors introduced by quantization propagate in two directions, i) to the next layers, like feedforward networks ii) across timesteps. Furthermore, RNN cells are

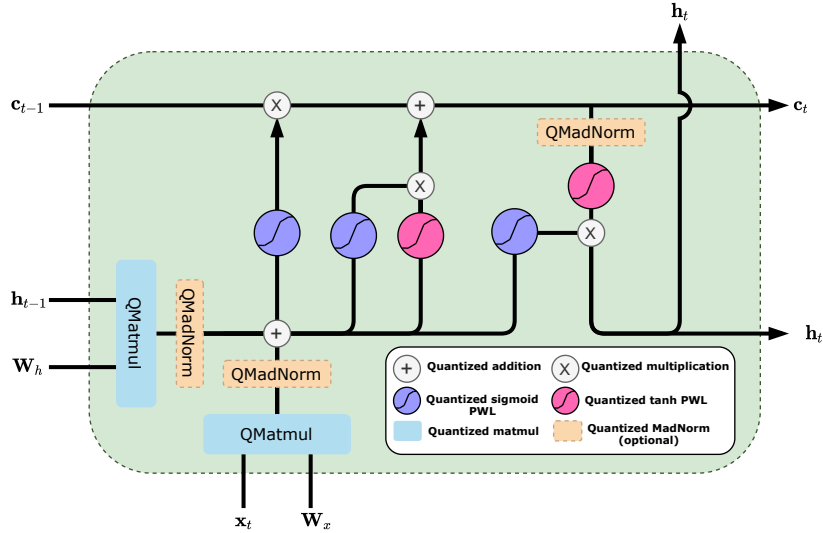


Figure 1: Example of an integer-only LSTM cell (iLSTM). Layer normalization change to quantized integer friendly MadNorm (QMadNorm), full-precision matrix multiplications change to integer matrix multiplication (QMatmul), sigmoid and tanh activations are replaced with their corresponding piecewise linear (PWL) approximations. See Figure 5 for a bigger size image.

computationally more complex; they include several element-wise additions and multiplications. They also have different activation functions that rely on the exponential function, such as sigmoid and hyperbolic tangent (tanh).

Accurate fully-integer RNNs calls for a new cell that is built using integer friendly operations. Our main motivation is to enable integer-only inference of RNNs on specialized AI computing hardware with no floating-point units, so we constrained the new LSTM cell to include only integer operations.

First we build a fully integer LSTM cell in which its inference require integer-only computation units, see Figure 1. Our method can be applied to any RNN architecture, but here we focus on LSTM networks which are the most commonly used RNNs.

Our contributions can be summarized as

- providing a quantization-aware piecewise linear approximation algorithm to replace exponential-based activation functions (e.g. sigmoid and tanh) with integer-friendly activation §4.1,
- introducing an integer-friendly normalization layer based on mean absolute deviation §4.2,
- proposing integer-only attention §4.3,
- wrapping up these new modules into an LSTM cell towards an integer-only LSTM cell §4.4.

2 Related Work

With ever-expanding deep models, designing efficient neural networks enable wider adoption of deep learning in industry. Researchers recently started working on developing various neural compression techniques. These techniques can be divided in four categories i) pruning (Luo et al., 2017; Ramakrishnan et al., 2020), ii) factorization (Denton et al., 2014; Hashemizadeh et al., 2020), iii) knowledge distillation (Hinton et al., 2015; Jafari et al., 2021) and iv) quantization (Jacob et al., 2017; Hubara et al., 2018; Darabi et al., 2018; Esser et al., 2020). Ott et al. (2016) explores low-bit quantization of weights for RNNs. They show binarizing weights lead to a massive accuracy drop, but ternarizing them keeps the model performance. Hubara et al. (2018) demonstrate quantizing RNNs to extremely low bits is challenging; they quantize weights and matrix product to 4-bit, but other operations such as element-wise pairwise and activations are computed in full-precision. Hou et al. (2019) quantize LSTM weights to 1-bit and 2-bit and show empirically that low-bit quantized LSTMs suffer from exploding gradients. Gradient explosion can be alleviated using normalization layers and leads to successful training of low bit weights Ardakani et al. (2018). Sari and Nia (2020) studied the effect of normalization in low bit networks theoretically, and proved that low-bit training without normalization operation is mathematically impossible; their work demonstrates the fundamental importance of involving

normalization layers in quantized networks. He et al. (2016) introduce Bit-RNN and improve 1-bit and 2-bit RNNs quantization by constraining values within fixed range carefully; they keep activation computation and element-wise pairwise operations in full-precision. Kapur et al. (2017) build upon Bit-RNN and propose a low-bit RNN with minimal performance drop, but they increase the number of neurons to compensate for performance drop; they run activation and pair-wise operations on full-precision as well.

Wu et al. (2016) is a pioneering work in LSTM quantization, which demonstrated speed-up inference of large-scale LSTM models with limited performance drop by partially quantizing RNN cells. Their proposed method is tailored towards specific hardware. They use 8-bit integer for matrix multiplications and 16-bit integer for tanh, sigmoid, and element-wise operations but do not quantize attention. Bluche et al. (2020) propose an effective 8-bit integer-only LSTM cell for Keyword Spotting application on microcontrollers. They enforce weights and activations to be symmetric on fixed ranges $[-4, 4]$ and $[-1, 1]$. This prior assumption about the network’s behaviour restricts generalizing their approach for wide range of RNN models. They propose a look-up table of 256 slots to represent the quantized tanh and sigmoid activations. However, the look-up table memory requirement explodes for bigger bitwidth. Their solution does not serve complex tasks such as automatic speech recognition due to large look up table memory consumption. While demonstrating strong results on Keyword Spotting task, their assumptions on quantization range and bitwidth make their method task-specific.

3 Background

We use the common linear algebra notation and use plain symbols to denote scalar values, e.g. $x \in \mathbb{R}$, bold lower-case letters to denote vectors, e.g. $\mathbf{x} \in \mathbb{R}^n$, and bold upper-case letters to denote matrices, e.g. $\mathbf{X} \in \mathbb{R}^{m \times n}$. The element-wise multiplication is represented by \odot .

3.1 LSTM

We define an LSTM cell as

$$\begin{pmatrix} \mathbf{i}_t \\ \mathbf{f}_t \\ \mathbf{j}_t \\ \mathbf{o}_t \end{pmatrix} = \mathbf{W}_x \mathbf{x}_t + \mathbf{W}_h \mathbf{h}_{t-1}, \quad (1)$$

$$\mathbf{c}_t = \sigma(\mathbf{f}_t) \odot \mathbf{c}_{t-1} + \sigma(\mathbf{i}_t) \odot \tanh(\mathbf{j}_t), \quad (2)$$

$$\mathbf{h}_t = \sigma(\mathbf{o}_t) \odot \tanh(\mathbf{c}_t), \quad (3)$$

where $\sigma(\cdot)$ is the sigmoid function; n is the input hidden units dimension, and m is the state hidden units dimension; $\mathbf{x}_t \in \mathbb{R}^n$ is the input for the current timestep $t \in \{1, \dots, T\}$; $\mathbf{h}_{t-1} \in \mathbb{R}^m$ is the hidden state from the previous timestep and \mathbf{h}_0 is initialized with zeros; $\mathbf{W}_x \in \mathbb{R}^{4m \times n}$ is the input to state weight matrix; $\mathbf{W}_h \in \mathbb{R}^{4m \times m}$ is the state to state weight matrix; $\{\mathbf{i}_t, \mathbf{f}_t, \mathbf{o}_t\} \in \mathbb{R}^m$ are the pre-activations to the {input, forget, output} gates; $\mathbf{j}_t \in \mathbb{R}^m$ is the pre-activation to the cell candidate; $\{\mathbf{c}_t, \mathbf{h}_t\} \in \mathbb{R}^m$ are the cell state and the hidden state for the current timestep, respectively. We omit the biases for the sake of notation simplicity. Bidirectional RNNs process the input sequence from left to right and right to left via a forward RNN, and a backward RNN. This allows to gather more context about the sequence Schuster and Paliwal (1997). For a bidirectional LSTM (BiLSTM) the output hidden state at timestep t is the concatenation of the forward hidden state $\vec{\mathbf{h}}_t$ and the backward hidden state $\overleftarrow{\mathbf{h}}_t$, $[\vec{\mathbf{h}}_t; \overleftarrow{\mathbf{h}}_t]$.

3.2 LayerNorm

Layer normalization Ba et al. (2016) standardizes inputs across the hidden units dimension with zero location and unit scale. Given hidden units $\mathbf{x} \in \mathbb{R}^H$, LayerNorm is defined as

$$\mu = \frac{1}{H} \sum_{i=1}^H x_i, \quad \hat{x}_i = x_i - \mu \quad (4)$$

$$\sigma_{\text{std}}^2 = \frac{1}{H} \sum_{i=1}^H \hat{x}_i^2, \quad \sigma_{\text{std}} = \sqrt{\sigma_{\text{std}}^2} \quad (5)$$

$$\text{LN}(\mathbf{x})_i = y_i = \frac{\hat{x}_i}{\sigma_{\text{std}}} \quad (6)$$

where μ (4) is the hidden unit mean, \hat{x}_i (4) is the centered hidden unit x_i , σ_{std}^2 (5) is the hidden unit variance, and y_i (6) is the normalized hidden unit. In practice, one can scale y_i by a learnable parameter γ or shift by a learnable parameter β . The LayerNormLSTM cell is defined as in Ba et al. (2016),

$$\begin{pmatrix} \mathbf{i}_t \\ \mathbf{f}_t \\ \mathbf{j}_t \\ \mathbf{o}_t \end{pmatrix} = \text{LN}(\mathbf{W}_x \mathbf{x}_t) + \text{LN}(\mathbf{W}_h \mathbf{h}_{t-1}), \quad (7)$$

$$\mathbf{c}_t = \sigma(\mathbf{f}) \odot \mathbf{c}_{t-1} + \sigma(\mathbf{i}) \odot \tanh(\mathbf{j}), \quad (8)$$

$$\mathbf{h}_t = \sigma(\mathbf{o}) \odot \tanh(\text{LN}(\mathbf{c}_t)), \quad (9)$$

with $H = 4m$ in (7) and $H = m$ in (9).

3.3 Attention

Attention is often used in encoder-decoder RNN architectures (Bahdanau et al., 2015; Chorowski et al., 2015; Wu et al., 2016). We employ Bahdanau attention, also called additive attention (Bahdanau et al., 2015). The attention mechanism allows the decoder network to attend to the variable-length output states from the encoder based on their relevance to the current decoder timestep. At each of its timesteps, the decoder extracts information from the encoder’s states and summarizes it as a context vector,

$$\mathbf{s}_t = \sum_{i=1}^{T_{\text{enc}}} \alpha_{ti} \odot \mathbf{h}_{\text{enc}_i} \quad (10)$$

$$\alpha_{ti} = \frac{\exp(e_{ti})}{\sum_{j=1}^{T_{\text{enc}}} \exp(e_{tj})} \quad (11)$$

$$e_{ti} = \mathbf{v}^\top \tanh(\mathbf{W}_q \mathbf{h}_{t-1} + \mathbf{W}_k \mathbf{h}_{\text{enc}_i}) \quad (12)$$

where \mathbf{s}_t is the context at decoder timestep t which is a weighted sum of the encoder hidden states outputs $\mathbf{h}_{\text{enc}_i} \in \mathbb{R}^{m_{\text{enc}}}$ along encoder timesteps $i \in \{1, \dots, T_{\text{enc}}\}$; $0 < \alpha_{ti} < 1$ are the attention weights attributed to each encoder hidden states based on the alignments $e_{ti} \in \mathbb{R}$; m_{dec} and m_{enc} are respectively the decoder and encoder hidden state dimension; $\{\mathbf{W}_q \in \mathbb{R}^{m_{\text{att}} \times m_{\text{dec}}}, \mathbf{W}_k \in \mathbb{R}^{m_{\text{att}} \times m_{\text{enc}}}\}$ are the weights matrices of output dimension m_{att} respectively applied to the query \mathbf{h}_{t-1} and the keys $\mathbf{h}_{\text{enc}_i}$; $\mathbf{v} \in \mathbb{R}^{m_{\text{att}}}$ is a learned weight vector. The context vector is incorporated into the LSTM cell by modifying (1) to

$$\begin{pmatrix} \mathbf{i} \\ \mathbf{f} \\ \mathbf{j} \\ \mathbf{o} \end{pmatrix} = \mathbf{W}_x \mathbf{x}_t + \mathbf{W}_h \mathbf{h}_{t-1} + \mathbf{W}_s \mathbf{s}_t \quad (13)$$

where $\mathbf{W}_s \in \mathbb{R}^{4m_{\text{dec}} \times m_{\text{enc}}}$.

3.4 Quantization

Quantization is a process whereby an input set is mapped to a lower resolution discrete set, called the quantization set \mathcal{Q} . The mapping is either performed from floating-points to integers (e.g. float32 to int8) or from a dense integer to another integer set with lower cardinality, e.g. int32 to int8. While elements from the quantized set are not required to exhibit a particular relationship, we would like the quantization process to be fast and readily implementable on a wide range of hardware. Therefore, we focus our work on uniform quantization. In a uniform quantization process, the distance between an element in the set and its subsequent element is always fixed and is called the step-size. This property enables us to map our implementation to hardware efficiently. The uniform quantization process can be implemented using readily available rounding, multiplication, and addition operators. We follow the quantization scheme described in Jacob et al. (2017). Detailed explanations and examples about quantization are given in Appendix A.2.

Given $x \in [x_{\min}, x_{\max}]$, we define the quantization process as

$$q_x = q(x) = \left\lfloor \frac{x}{S_x} \right\rfloor + Z_x \quad (14)$$

$$r_x = r(x) = S_x (q_x - Z_x) \quad (15)$$

$$S_x = \frac{x_{\max} - x_{\min}}{2^b - 1}, \quad Z_x = \left\lfloor \frac{-x_{\min}}{S_x} \right\rfloor \quad (16)$$

where the input is clipped between x_{\min} and x_{\max} beforehand; $\lfloor \cdot \rfloor$ is the round-to-nearest function; S_x is the scaling factor (also known as the step-size); b is the bitwidth, e.g. $b = 8$ for 8-bit quantization, $b = 16$ for 16-bit quantization; Z_x is the zero-point corresponding to the quantized value of 0 (note that zero should always be included in $[x_{\min}, x_{\max}]$); $q(x)$ quantize x to an integer number and $r(x)$ gives the floating-point value $q(x)$ represents, i.e. $r(x) \approx x$. We refer to $\{x_{\min}, x_{\max}, b, S_x, Z_x\}$ as **quantization parameters** of x . Note that for inference, S_x is expressed as a fixed-point integer number rather than a floating-point number, allowing for integer-only arithmetic computations (Jacob et al. 2017, Appendix A.2.6).

We perform Quantization-Aware Training (QAT), in which the quantization effects are simulated during training to let the network adapt to the quantization error. Simulating quantization is done via Fake Quantization where a floating-point value is first quantized, then dequantized to the corresponding floating-point value in the quantization set. The fake quantization function is a non-differentiable operation; therefore we set its derivative to be the straight-through estimator (STE) (Hinton, 2012)

$$\text{fakequant}(x) = r(x), \quad \text{fakequant}'(x) = 1 \quad (17)$$

For a weight matrix, the quantization range x_{\min} and x_{\max} are respectively the minimum and maximum values within the matrix. We use symmetric quantization as weight distributions are typically symmetric around zero and would enable better speedups at inference time. Activations, on the other hand, are dynamic; thus, we keep track of a moving average of their minimum and maximum values as described in Jacob et al. (2017).

There are a set of rules to follow to map a model to integer-only operations correctly; see Appendix A.2.1 for more details. All constants involving floating-point values (e.g. scaling factors) can be expressed as integer fixed-point multipliers. Therefore no floating-points operations are required at inference, see Appendix A.2.6 and for further details, see Appendix A.2.

4 Methodology

In this section, we describe our task-agnostic quantization-aware training method to enable integer-only RNN (iRNN).

4.1 Integer-only activation

First, we need to compute activation functions without relying on floating-point operations to take the early step towards an integer-only RNN. At inference, the non-linear activation is applied to the quantized input q_x , performs operations using integer-only arithmetic and outputs the quantized result q_y . Clearly, given the activation function f , $q_y = q(f(q_x))$; as the input and the activation output are both quantized, we obtain a discrete mapping from q_x to q_y . There are several ways to formalize this operation. The first solution is a Look-Up Table (LUT), where q_x is the index and $q_y = \text{LUT}[q_x]$. Thus, the number of slots in the LUT is 2^b (e.g. 256 bytes for $b = 8$ bits input q_x). This method does not scale to large indexing bitwidths, e.g. 65536 slots need to be stored in memory for 16-bit activation quantization. LUT is not cache-friendly for large numbers of slots. The second solution is approximating the full-precision activation function using a fixed-point integer Taylor approximation, but the amount of computations grows as the approximation order grows. We propose to use a **Quantization-Aware PWL** that selects PWL knots during the training process to produce the linear pieces. Therefore the precision of approximation adapts to the required range of data flow automatically and provides highly accurate data-dependent activation approximation with fewer pieces.

A PWL is defined as follows,

$$g(x) = \sum_{i=1}^N \mathbb{1}_{[k_i, k_{i+1})} (a_i(x - k_i) + b_i), \quad (18)$$

where N is the number of linear pieces defined by $N + 1$ knots (also known as cutpoints or breakpoints); $\{a_i, k_i, b_i = f(k_i)\}$ are the slope, the knot, and the intercept of the i^{th} piece respectively; $\mathbb{1}_A(x) = 1$ is the indicator function on A . The more the linear pieces, the better the activation approximation is (see Figure 2). A PWL is suitable for simple fixed-point integer operations. It only relies on basic arithmetic operations and is easy to parallelize because the computation of each piece is independent. Therefore, the challenge is to select the knot locations that provide the best PWL approximation to the original function f . Note in this regime, we only approximate the activation function on the subset corresponding quantized inputs and not the whole full-precision range. In our proposed method if $x = k_i$ then $g(x) = g(k_i) = b_i$, i.e. recovers the exact output $f(k_i)$. Hence, if the PWL has 2^b knots (i.e. $2^b - 1$ pieces), it is equivalent to a look-up table representing the quantized activation function. Thus, we constraint the knots to be a subset of the quantized inputs of the function we are approximating (i.e. $\{k_i\}_{i=1}^{N+1} \subseteq \mathcal{Q}$).

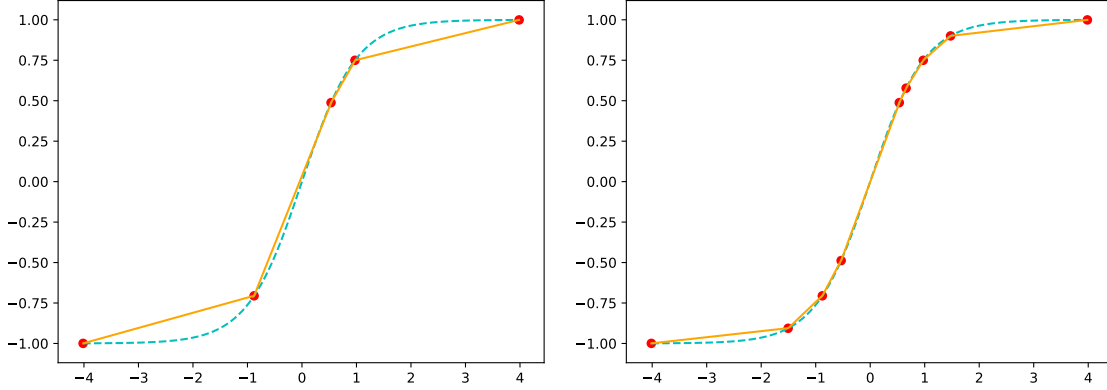


Figure 2: Tanh approximations using quantization-aware PWLs with 4 knots (left panel), 16 pieces (right panel) using (18). The dashed cyan curves are the true tanh functions, while the solid orange curves are its approximation from Algorithm (1). Red dots are the knots. The more we add pieces, the better the approximation is. Our algorithm is able to prioritize sections of the function with more curvatures. See Figure 3.

We propose a recursive greedy algorithm to locate the knots during the quantization-aware PWL. The algorithm starts with $2^b - 1$ pieces and recursively removes one knot at a time until it reaches the specified number of pieces. The absolute differences between adjacent slopes are computed, and the shared knot from the pair of slopes that minimizes the absolute difference is removed; see Figure 4. The algorithm is simple to implement and applied only once at a given training step; see Algorithm 1. This algorithm is linear in time and space complexity with respect to the number of starting pieces and is generic to cover various nonlinear functions, see Figure 3. Note that the PWL is specific to a given set of quantization parameters, i.e. the quantization parameters are kept frozen after its creation.

At inference, the quantization-aware PWL is computed as follows

$$q_y = \left[\sum_{i=1}^N \mathbb{1}_{[q_{k_i}, q_{k_{i+1}})} \left(\frac{S_x a_i}{S_y} (q_x - q_{k_i}) + \frac{b_i}{S_y} \right) \right] + Z_y,$$

where the constants are expressed as fixed-point integers; see Appendix A.2.6.

4.2 Integer-only normalization

Normalization greatly helps the convergence of quantized networks (Hou et al., 2019; Sari and Nia, 2020). There is a plurality of measures of location and scale to define normalization operation. The commonly used measure of dispersion is the standard deviation to define normalization, which is imprecise and costly to compute on integer-only hardware. However, the mean absolute deviation (MAD) is integer-friendly and defined as

$$d = \frac{1}{H} \sum_{i=1}^H |x_i - \mu| = \frac{1}{H} \sum_{i=1}^H |\hat{x}_i|. \quad (19)$$

While the mean minimizes the standard deviation, the median minimizes MAD. We suggest measuring deviation with respect to mean for two reasons: i) the median is computationally more expensive ii) the absolute deviation from the mean is closer to the standard deviation. For Gaussian data, the MAD is $\approx 0.8\sigma_{\text{std}}$ so that it might be exchanged with standard deviation. We propose to LayerNorm in LSTM with MAD instead of standard deviation and refer to it as MadNorm., where (6) is replaced by

$$y_i = \frac{\hat{x}_i}{d}. \quad (20)$$

MadNorm involves simpler operations, as there is no need to square and no need to take the square root while taking absolute value instead of these two operations is much cheaper. The values $\{\mu, \hat{x}_i, d, y_i\}$ are 8-bit quantized and

computed as follows

$$q_\mu = \left\lfloor \frac{S_x}{S_\mu N} \left(\sum_{i=1}^N q_{x_i} - N Z_x \right) \right\rfloor + Z_\mu, \quad (21)$$

$$q_{\hat{x}_i} = \left\lfloor \frac{S_x}{S_{\hat{x}}} (q_{x_i} - Z_x) - \frac{S_\mu}{S_{\hat{x}}} (q_\mu - Z_\mu) \right\rfloor + Z_{\hat{x}}, \quad (22)$$

$$q_d = \left\lfloor \frac{S_{\hat{x}}}{S_d N} \sum_{i=1}^N |q_{\hat{x}_i} - Z_{\hat{x}}| \right\rfloor + Z_d, \quad (23)$$

$$q_{y_i} = \left\lfloor \frac{\frac{S_{\hat{x}}}{S_y S_d} (q_{\hat{x}_i} - Z_{\hat{x}})}{\max(q_d, 1)} \right\rfloor + Z_y, \quad (24)$$

where all floating-point constants can be expressed as fixed-point integer numbers, allowing for integer-only arithmetic computations. Note that (21-24) are only examples of ways to perform integer-only arithmetic for MadNorm, and may change depending on the software implementation and the target hardware.

4.3 Integer-only attention

Attention plays a crucial role in modern encoder-decoder architectures. The decoder relies on attention to extract information from the encoder and provide predictions. Attention is the bridge between the encoder and the decoder. Careless quantization of attention breaks apart the decoder due to quantization noise.

We propose to quantize $\{\mathbf{v}, \mathbf{W}_q, \mathbf{W}_k\}$ to 8-bit. The vectors \mathbf{h}_{t-1} and $\mathbf{h}_{\text{enc}_i}$ are quantized thank to §4.1 and 4.2. The matrix multiplications in (12) are performed in 8-bit and their results are quantized to 8-bit, each with their own quantization parameters. Since those matrix multiplications do not share the same quantization parameters, the sum (12) require proper rescaling following (27), and the result is quantized to 16-bit. We found 8-bit quantization adds too much noise, thus preventing the encoder-decoder model to work correctly. The tanh function in (12) is computed using quantization-aware PWL and its outputs are quantized to 8-bit. The alignments e_{ti} are quantized to 16-bit (12). The exponential function in α_{ti} is computed using a quantization-aware PWL, with its outputs quantized to 8-bit. We found that quantizing the softmax denominator (11) to 8-bit introduces too much noise and destroys attention. 8-bit attention does not offer enough flexibility and prevents fine grained decoder attention to the encoder. We left the denominator in 32-bit integer value and defer quantization to 8-bit in the division. The context vector \mathbf{s}_t is quantized to 8-bit. Note that in practice we shift the inputs to softmax for numerical stability reasons (i.e. $e_{ti} - \max_j e_{tj}$).

4.4 Integer-only LSTM network

A vanilla LSTM cell comprises matrix multiplications, element-wise additions, element-wise multiplications, tanh, and sigmoid activations (1 - 3). We quantize the weights matrices \mathbf{W}_x and \mathbf{W}_h to 8-bit. The inputs \mathbf{x}_t and hidden states \mathbf{h}_{t-1} are already 8-bit quantized from the previous layer and from the previous timestep. The cell states \mathbf{c}_t are theoretically unbounded (2); therefore the amount of quantization noise potentially destroys the information carried by \mathbf{c}_t , if it spans a large range. When performing QAT on some pre-trained models, it is advised to quantize \mathbf{c}_t to 16-bit. Therefore, \mathbf{c}_t is 8-bit quantized unless stated otherwise but can be quantized to 16-bit if necessary. Matrix multiplications in (1) are performed with 8-bit arithmetic, and their outputs are quantized to 8-bit based on their respective quantization parameters. The sum between the two matrix multiplications outputs in (1) are performed following (27), because they do not share the same quantization parameters, see Appendix A.2.5. The results of the sum are quantized to 8-bit; however, 16-bit quantization might be necessary for complex tasks. The sigmoid and tanh activations in (2) and (3) are replaced with their own quantization-aware PWL, and their output is always quantized to 8-bit. The element-wise multiplications operations are distributive, and sharing quantization parameters is not required. In (2), the element-wise multiplications are quantized to 8-bit, but can be quantized to 16-bit if \mathbf{c}_t is quantized to 16-bit as well; the element-wise additions are quantized based on \mathbf{c}_t 's bitwidth (i.e. 8-bit or 16-bit).

The element-wise multiplications between sigmoid and tanh in (3) is always quantized to 8-bit, because \mathbf{h}_t are always quantized to 8-bit. Following this recipe, we obtain an integer-only arithmetic LSTM cell, see Figure. 1. For LSTM cells with LayerNorm §3.2) quantized MadNorm layers are used instead of LayerNorm (4.2). Appendix A.1 provides details about quantization of other types of layers in an LSTM model.

LayerNorm LSTM	val	test
Full-precision	98.58 \pm 0.35	94.84 \pm 0.21
iRNN w/ PWL4	101.40 \pm 0.70	98.11 \pm 0.75
iRNN w/ PWL8	98.14 \pm 0.11	95.03 \pm 0.16
iRNN w/ PWL16	98.09 \pm 0.06	94.92 \pm 0.05
iRNN w/ PWL32	97.97 \pm 0.01	94.81 \pm 0.02

Table 1: Word-level perplexities on PTB with a LayerNorm LSTM and quantized models with a different number of PWL pieces. LayerNorm is replaced with MadNorm (§4.2) for the quantized models (iRNN). Best results are averaged across 3 runs \pm standard deviation.

Mogrifier LSTM	val	test
Full-precision	60.27 \pm 0.34	58.02 \pm 0.34
iRNN w/ PWL8	60.91 \pm 0.04	58.54 \pm 0.07
iRNN w/ PWL16	60.65 \pm 0.09	58.21 \pm 0.08
iRNN w/ PWL32	60.37 \pm 0.03	57.93 \pm 0.07

Table 2: Word-level perplexities on WikiText2 with Mogrifier LSTM and quantized models with different number of PWL pieces. Best results are averaged across 3 runs \pm standard deviations.

5 Experiments

We evaluate our proposed method, iRNN, on language modeling and automatic speech recognition. We also implemented our approach on a smartphone to benchmark inference speedup, see Appendix A.4.

5.1 Language modeling on PTB

As a proof of concept, we perform several experiments on full-precision and fully 8-bit quantized models on the Penn TreeBank (PTB) dataset (Marcus et al., 1993). We report perplexity per word as a performance metric.

For the quantized models, the LayerNorm is replaced with MadNorm. We do not train full-precision models with MadNorm to make our method comparable with common full-precision architectures. However, comparing MadNorm to LayerNorm in the full-precision setting shows that MadNorm gives a similar performance (Table 7). We can draw two conclusions from the results presented in Table 1, i) replacing LayerNorm by MadNorm does not destroy model performance, ii) using eight linear pieces is enough to retain the performance of the model, but adding more linear pieces improves the performance. We could obtain even superior results in the quantized model compared to the full-precision model because of the regularization introduced by quantization errors.

5.2 Language modeling on WikiText2

We evaluated our proposed method on the WikiText2 dataset (Merity et al., 2016) with a state-of-the-art RNN, Mogrifier LSTM (Melis et al., 2020). The original code¹ was written in TensorFlow, we reimplemented our own version in PyTorch by staying as close as possible to the TensorFlow version. We follow the experimental setup from the authors² as we found it critical to get similar results. We use a two layer Mogrifier LSTM. The setup and hyper-parameters for the experiments can be found in Appendix A.3.2 to save some space. We present our results averaged over 3 runs in Table 2. We use the best full-precision model, which scores 59.95 perplexity to initialize the quantized models. Our method is able to produce 8-bit quantized integer-only Mogrifier LSTM with similar performance to the full-precision model with only about 0.3 perplexity increase for the quantized model with a PWL of 32 pieces and a maximum of about 0.9 perplexity increase with a number of pieces as low as 8. Interestingly, a pattern emerged by doubling the number of pieces, as we get a decrease in perplexity by about 0.3. We also perform a thorough ablation study of our method (Table 6), details can be found in Appendix A.3.2. Surprisingly, we found that stochastic weight averaging for quantized models exhibits the same behavior as for full-precision models and improved performance thanks to regularization. While experiments on the PTB dataset were a demonstration of the potential of our method, these experiments on WikiText2 show that our proposed method is able to stay on par with state-of-the-art RNN models.

¹<https://github.com/deepmind/lamb>

²https://github.com/deepmind/lamb/blob/254a0b0e330c44e00cf535f98e9538d6e735750b/lamb/experiment/mogrifier/config/c51c838b33a5+_tune_wikitext-2_35m_lstm_mos2_fm_d2_arms/trial_747/config

ESPRESSO LSTM	set	clean	other
Full-precision	dev	2.99	8.77
iRNN w/ PWL96*	dev	3.73	10.02
Full-precision	test	3.37	9.49
iRNN w/ PWL96*	test	4.11	10.71

Table 3: WER% on LibriSpeech with ESPRESSO LSTM (Encoder-Decoder LSTM with Attention) with LM shallow fusion. *(160 pieces were used for the exponential function)

5.3 ASR on LibriSpeech

We experiment on an ASR task based on the setup of Wang et al. (2019b) and their ESPRESSO framework³. We used an LSTM-based Attention Encoder-Decoder (ESPRESSO LSTM) trained on the LibriSpeech dataset (Panayotov et al., 2015). Experiments setup and hyper-parameters are provided in Appendix A.3.3. We initialize the quantized model from the pre-trained full-precision ESPRESSO LSTM. In our early experiments, we found that quantizing the model to 8-bit would not give comparable results. After investigation, we noticed it was mainly due to two reasons, i) the cell states c_t had large ranges (e.g. $[-17, 15]$), ii) the attention mechanism was not letting the decoder attend the encoder outputs accurately. Therefore, we quantize the pre-activation gates (1), the element-wise multiplications in (2) and cell states c_t to 16-bit. The attention is quantized following §4.3. Everything else is quantized to 8-bit following §4.4. The number of pieces for the quantization-aware PWLs is 96, except for the exponential function in the attention, which is 160 as we found out it was necessary to have more pieces because of its curvature. The number of pieces used is higher than in the language modeling experiments we did. However, the difference is that the inputs to the activation functions are 16-bit rather than 8-bit although the outputs are still quantized to 8-bit. It means we need more pieces to capture the inputs resolution better. Note that it would not be feasible to use a 16-bit Look-Up Table to compute the activation functions due to the size and cache misses, whereas using 96 pieces allows for a 170x reduction in memory consumption compared to LUT. The quantized model has a similar performance to the full-precision model, with a maximum of 1.25 WER% drop (Table 3). We believe allowing the model to train longer would reduce the gap.

6 Conclusion

We propose a task-agnostic and flexible methodology to enable integer-only RNNs. To the best of our knowledge, we are the first to offer an approach to quantize all existing operations in modern RNNs, supporting normalization and attention. We evaluated our approach on high-performance LSTM-based models on language modeling and ASR, which have distinct architectures and variable computation requirements. We show that RNN can be fully quantized while achieving similar performance as their full-precision counterpart. We benchmark our method on a smartphone, where we obtain $2\times$ inference speedup and $4\times$ memory reduction. This allows to deploy a wide range of RNN architectures on specialized AI hardware and microcontrollers that lack floating point operation.

References

- Arash Ardakani, Zhengyun Ji, Sean C Smithson, Brett H Meyer, and Warren J Gross. 2018. Learning recurrent binary/ternary weights. *arXiv preprint arXiv:1809.11086*.
- Jimmy Ba, Jamie Ryan Kiros, and Geoffrey E. Hinton. 2016. Layer normalization. *ArXiv*, abs/1607.06450.
- Dzmitry Bahdanau, Kyunghyun Cho, and Yoshua Bengio. 2015. Neural machine translation by jointly learning to align and translate. In *3rd International Conference on Learning Representations, ICLR 2015, San Diego, CA, USA, May 7-9, 2015, Conference Track Proceedings*.
- Théodore Bluche, Maël Primet, and Thibault Gisselbrecht. 2020. Small-footprint open-vocabulary keyword spotting with quantized lstm networks. *arXiv preprint arXiv:2002.10851*.
- Mia Xu Chen, Orhan Firat, Ankur Bapna, Melvin Johnson, Wolfgang Macherey, George Foster, Llion Jones, Mike Schuster, Noam Shazeer, Niki Parmar, Ashish Vaswani, Jakob Uszkoreit, Lukasz Kaiser, Zhifeng Chen, Yonghui Wu, and Macduff Hughes. 2018. The best of both worlds: Combining recent advances in neural machine translation. In *Proceedings of the 56th Annual Meeting of the Association for Computational Linguistics (Volume 1: Long Papers)*, pages 76–86, Melbourne, Australia. Association for Computational Linguistics.
- Kyunghyun Cho, Bart Van Merriënboer, Dzmitry Bahdanau, and Yoshua Bengio. 2014. On the properties of neural machine translation: Encoder-decoder approaches. *arXiv preprint arXiv:1409.1259*.

³<https://github.com/freewym/espresso>

- Jan Chorowski, Dzmitry Bahdanau, Dmitriy Serdyuk, Kyunghyun Cho, and Yoshua Bengio. 2015. Attention-based models for speech recognition. *arXiv preprint arXiv:1506.07503*.
- Sajad Darabi, Mouloud Belbahri, Matthieu Courbariaux, and Vahid Partovi Nia. 2018. BNN+: improved binary network training. *CoRR*, abs/1812.11800.
- Emily L Denton, Wojciech Zaremba, Joan Bruna, Yann LeCun, and Rob Fergus. 2014. Exploiting linear structure within convolutional networks for efficient evaluation. In *Advances in Neural Information Processing Systems*, volume 27. Curran Associates, Inc.
- Jacob Devlin, Ming-Wei Chang, Kenton Lee, and Kristina Toutanova. 2019. BERT: Pre-training of deep bidirectional transformers for language understanding. In *Proceedings of the 2019 Conference of the North American Chapter of the Association for Computational Linguistics: Human Language Technologies, Volume 1 (Long and Short Papers)*, pages 4171–4186, Minneapolis, Minnesota. Association for Computational Linguistics.
- Steven K. Esser, Jeffrey L. McKinstry, Deepika Bablani, Rathinakumar Appuswamy, and Dharmendra S. Modha. 2020. Learned step size quantization. In *ICLR*. OpenReview.net.
- Yarin Gal and Zoubin Ghahramani. 2016. A theoretically grounded application of dropout in recurrent neural networks. In *Advances in Neural Information Processing Systems*, volume 29. Curran Associates, Inc.
- Meraj Hashemizadeh, Michelle Liu, Jacob Miller, and Guillaume Rabusseau. 2020. Adaptive tensor learning with tensor networks. *arXiv preprint arXiv:2008.05437*.
- Qinyao He, He Wen, Shuchang Zhou, Yuxin Wu, Cong Yao, Xinyu Zhou, and Yuheng Zou. 2016. Effective quantization methods for recurrent neural networks. *arXiv preprint arXiv:1611.10176*.
- Yanzhang He, Tara N Sainath, Rohit Prabhavalkar, Ian McGraw, Raziell Alvarez, Ding Zhao, David Rybach, Anjuli Kannan, Yonghui Wu, Ruoming Pang, et al. 2019. Streaming end-to-end speech recognition for mobile devices. In *ICASSP 2019-2019 IEEE International Conference on Acoustics, Speech and Signal Processing (ICASSP)*, pages 6381–6385. IEEE.
- Dan Hendrycks and Kevin Gimpel. 2016. Gaussian error linear units (gelus). *arXiv preprint arXiv:1606.08415*.
- Geoffrey Hinton. 2012. Neural networks for machine learning. *Coursera*, video lectures.
- Geoffrey Hinton, Oriol Vinyals, and Jeff Dean. 2015. Distilling the knowledge in a neural network.
- Sepp Hochreiter and Jürgen Schmidhuber. 1997. Long short-term memory. *Neural Comput.*, 9(8):1735–1780.
- Lu Hou, Jinhua Zhu, James Tin-Yau Kwok, Fei Gao, Tao Qin, and Tie-yan Liu. 2019. Normalization helps training of quantized lstm.
- Itay Hubara, Matthieu Courbariaux, Daniel Soudry, Ran El-Yaniv, and Yoshua Bengio. 2018. Quantized neural networks: Training neural networks with low precision weights and activations. *Journal of Machine Learning Research*, 18(187):1–30.
- Pavel Izmailov, Dmitrii Podoprikin, Timur Garipov, Dmitry Vetrov, and Andrew Gordon Wilson. 2018. Averaging weights leads to wider optima and better generalization. *arXiv preprint arXiv:1803.05407*.
- Benoit Jacob, Skirmantas Kligys, Bo Chen, Menglong Zhu, Matthew Tang, Andrew G. Howard, Hartwig Adam, and Dmitry Kalenichenko. 2017. Quantization and training of neural networks for efficient integer-arithmetic-only inference. *2018 IEEE/CVF Conference on Computer Vision and Pattern Recognition*, pages 2704–2713.
- Aref Jafari, Mehdi Rezagholizadeh, Pranav Sharma, and Ali Ghodsi. 2021. Annealing knowledge distillation.
- Supriya Kapur, Asit Mishra, and Debbie Marr. 2017. Low precision rnns: Quantizing rnns without losing accuracy. *arXiv preprint arXiv:1710.07706*.
- Jungo Kasai, Hao Peng, Yizhe Zhang, Dani Yogatama, Gabriel Ilharco, Nikolaos Pappas, Yi Mao, Weizhu Chen, and Noah A Smith. 2021. Finetuning pretrained transformers into rnns. *arXiv preprint arXiv:2103.13076*.
- Diederik P. Kingma and Jimmy Ba. 2014. Adam: A method for stochastic optimization. *CoRR*, abs/1412.6980.
- Ben Krause, Emmanuel Kahembwe, Iain Murray, and Steve Renals. 2018. Dynamic evaluation of neural sequence models. In *Proceedings of the 35th International Conference on Machine Learning*, volume 80 of *Proceedings of Machine Learning Research*, pages 2766–2775. PMLR.
- Raghuraman Krishnamoorthi. 2018. Quantizing deep convolutional networks for efficient inference: A whitepaper. *arXiv preprint arXiv:1806.08342*.
- Jian-Hao Luo, Jianxin Wu, and Weiyao Lin. 2017. Thinet: A filter level pruning method for deep neural network compression. *CoRR*, abs/1707.06342.

- Mitchell P. Marcus, Beatrice Santorini, and Mary Ann Marcinkiewicz. 1993. Building a large annotated corpus of English: The Penn Treebank. *Computational Linguistics*, 19(2):313–330.
- Gábor Melis, Tomáš Kočiský, and Phil Blunsom. 2020. Mogrifier lstm. In *International Conference on Learning Representations*.
- Stephen Merity, Caiming Xiong, James Bradbury, and Richard Socher. 2016. Pointer sentinel mixture models. *CoRR*, abs/1609.07843.
- Tomáš Mikolov, Ilya Sutskever, Anoop Deoras, Hai-Son Le, Stefan Kombrink, and Jan Cernocky. 2012. Subword language modeling with neural networks. *preprint (http://www.fit.vutbr.cz/imikolov/rnnlm/char.pdf)*, 8:67.
- Joachim Ott, Zhouhan Lin, Ying Zhang, Shih-Chii Liu, and Yoshua Bengio. 2016. Recurrent neural networks with limited numerical precision. *arXiv preprint arXiv:1608.06902*.
- Vassil Panayotov, Guoguo Chen, Daniel Povey, and Sanjeev Khudanpur. 2015. Librispeech: an asr corpus based on public domain audio books. In *Acoustics, Speech and Signal Processing (ICASSP), 2015 IEEE International Conference on*, pages 5206–5210. IEEE.
- Adam Paszke, Sam Gross, Francisco Massa, Adam Lerer, James Bradbury, Gregory Chanan, Trevor Killeen, Zeming Lin, Natalia Gimelshein, Luca Antiga, Alban Desmaison, Andreas Kopf, Edward Yang, Zachary DeVito, Martin Raison, Alykhan Tejani, Sasank Chilamkurthy, Benoit Steiner, Lu Fang, Junjie Bai, and Soumith Chintala. 2019. Pytorch: An imperative style, high-performance deep learning library. In *Advances in Neural Information Processing Systems*, volume 32. Curran Associates, Inc.
- Ramchalam Kinattinkara Ramakrishnan, Eyyub Sari, and Vahid Partovi Nia. 2020. Differentiable mask for pruning convolutional and recurrent networks. In *2020 17th Conference on Computer and Robot Vision (CRV)*, pages 222–229. IEEE.
- D. Rumelhart, Geoffrey E. Hinton, and R. J. Williams. 1986. Learning internal representations by error propagation.
- Eyyüb Sari and Vahid Partovi Nia. 2020. Batch normalization in quantized networks. In *Proceedings of the Edge Intelligence Workshop*, pages 6–9.
- Mike Schuster and Kuldeep K Paliwal. 1997. Bidirectional recurrent neural networks. *IEEE transactions on Signal Processing*, 45(11):2673–2681.
- Christian Szegedy, Vincent Vanhoucke, Sergey Ioffe, Jon Shlens, and Zbigniew Wojna. 2016. Rethinking the inception architecture for computer vision. In *Proceedings of the IEEE conference on computer vision and pattern recognition*, pages 2818–2826.
- Ashish Vaswani, Noam Shazeer, Niki Parmar, Jakob Uszkoreit, Llion Jones, Aidan N Gomez, Łukasz Kaiser, and Illia Polosukhin. 2017. Attention is all you need. In I. Guyon, U. V. Luxburg, S. Bengio, H. Wallach, R. Fergus, S. Vishwanathan, and R. Garnett, editors, *Advances in Neural Information Processing Systems 30*, pages 5998–6008. Curran Associates, Inc.
- Chengyi Wang, Shuangzhi Wu, and Shujie Liu. 2019a. Accelerating transformer decoding via a hybrid of self-attention and recurrent neural network. *arXiv preprint arXiv:1909.02279*.
- Yiming Wang, Tongfei Chen, Hainan Xu, Shuoyang Ding, Hang Lv, Yiwen Shao, Nanyun Peng, Lei Xie, Shinji Watanabe, and Sanjeev Khudanpur. 2019b. Espresso: A fast end-to-end neural speech recognition toolkit. In *2019 IEEE Automatic Speech Recognition and Understanding Workshop (ASRU)*, pages 136–143.
- Paul J Werbos. 1990. Backpropagation through time: what it does and how to do it. *Proceedings of the IEEE*, 78(10):1550–1560.
- Yonghui Wu, Mike Schuster, Zhifeng Chen, Quoc V Le, Mohammad Norouzi, Wolfgang Macherey, Maxim Krikun, Yuan Cao, Qin Gao, Klaus Macherey, et al. 2016. Google’s neural machine translation system: Bridging the gap between human and machine translation. *arXiv preprint arXiv:1609.08144*.
- Zhilin Yang, Zihang Dai, Ruslan Salakhutdinov, and William W. Cohen. 2018. Breaking the softmax bottleneck: A high-rank rnn language model.

A Appendix

A.1 Specific details on LSTM-based models

For BiLSTM cells, nothing stated in §4.4 is changed except that we enforce the forward LSTM hidden state $\vec{\mathbf{h}}_t$ and the backward LSTM hidden state $\overleftarrow{\mathbf{h}}_t$ to share the same quantization parameters so that they can be concatenated as a vector. If the model has embedding layers, they are quantized to 8-bit as we found they were not sensitive to quantization. If the model has residual connections (e.g. between LSTM cells), they are quantized to 8-bit integers. In encoder-decoder models the attention layers would be quantized following §4.3. The model’s last fully-connected layer’s weights are 8-bit quantized to allow for 8-bit matrix multiplication. However, we do not quantize the outputs and let them remain 32-bit integers as often this is where it is considered that the model has done its job and that some postprocessing is performed (e.g. beam search).

A.2 Refresher on quantization

This section is intended for readers who are novices in model quantization and Jacob et al. (2017)’s work. For the examples, we focus on 8-bit quantization (i.e. $b = 8$) unless stated otherwise.

A.2.1 Rules about integer-only operations

We describe how to correctly map a model to integer-only operators for all element-wise multiplication and additions. Refer to Jacob et al. (2017) describes how to do this for matrix-multiplications and other operators. At inference, the inputs to any operation are already quantized. For the following explanations, we define two quantized inputs q_a with scaling factor S_a and zero-point Z_a , q_b with scaling factor S_b and zero-point Z_b . We also define q_c with scaling factor S_c and zero-point Z_c that will be the quantized output of the operations. Note that all the scaling factors and zero-point come from the set of quantization parameters determined during QAT. The multiplication operation does not require q_a and q_b to share quantization parameters, therefore it is defined as,

$$q_c = \left\lfloor \frac{S_a S_b}{S_c} (q_a q_b - q_a Z_b - q_b Z_a + Z_a Z_b) \right\rfloor + Z_c, \quad (25)$$

where the multiplication $q_a q_b$ is a b -bit multiplication (example given in Appendix A.2.4). Addition can take two forms based on the quantization parameters of q_a and q_b . If they share the same quantization parameters (i.e. $S_b = S_a$ and $Z_b = Z_a$), it can be computed as follows,

$$q_c = \left\lfloor \frac{S_a}{S_c} (q_a + q_b - 2Z_a) \right\rfloor + Z_c \quad (26)$$

where $q_a + q_b$ is a b -bit addition. However, if they do not share the same quantization parameters,

$$q_c = \left\lfloor \frac{S_a}{S_c} (q_a - Z_a) + \frac{S_b}{S_c} (q_b - Z_b) \right\rfloor + Z_c \quad (27)$$

rescaling q_a and q_b is needed, which means the addition has to be computed with more bitwidth, e.g. 32-bit (examples given in Appendix A.2.5). All constants involving floating-points values (e.g. scaling factors) can be expressed as integer fixed-point multipliers, therefore no floating-points operations are required at inference (Appendix A.2.6). Refer to Appendix A.2 for more information.

A.2.2 Computing scaling factor and zero-point

Given a range $[x_{\min}, x_{\max}]$, e.g. $[-1, 1]$ and a bitwidth b , e.g. 8; the scaling factor S_x and zero-point Z_x are computed as follow,

$$S_x = \frac{x_{\max} - x_{\min}}{2^b - 1} = \frac{2}{255} \approx 0.0078 \quad (28)$$

$$Z_x = \left\lfloor \frac{-x_{\min}}{S_x} \right\rfloor = \left\lfloor \frac{1}{S_x} \right\rfloor = 128. \quad (29)$$

To not clutter the writing, we will assume S_x exactly equals 0.0078. If $b = 16$, we are able to represent more numbers, i.e. the scaling factor will be smaller,

$$S_x = \frac{x_{\max} - x_{\min}}{2^b - 1} = \frac{2}{65535} \approx 3.05 \times 10^{-5} \quad (30)$$

$$Z_x = \left\lfloor \frac{-x_{\min}}{S_x} \right\rfloor = \left\lfloor \frac{1}{S_x} \right\rfloor = 32768. \quad (31)$$

A.2.3 Quantizing a floating-point number

Given a number within the previously defined range A.2.2, i.e. $x \in [-1, 1]$, and the scaling factor S_x (28) and zero-point Z_x (29), we can quantize it following (14). For instance, for $x = 0.2$,

$$q(x) = \left\lfloor \frac{x}{S_x} \right\rfloor + Z_x = \left\lfloor \frac{0.2}{0.0078} \right\rfloor + 128 = 154, \quad (32)$$

hence $q_x = 154$. The corresponding floating-point representation of q_x , r_x , is

$$r(x) = S_x(q_x - Z_x) \quad (33)$$

$$= 0.0078(154 - 128) = 0.2028. \quad (34)$$

Hence, after quantizing the floating-point value 0.2, its dequantized value is 0.2028, so the error introduced is $\epsilon = |x - r_x| = 0.0028$. The purpose of QAT with fake quantization (17) is to try to force the network to be insensitive to noise introduced by these ϵ errors. The error introduced by quantization is bounded by is $\epsilon \leq \frac{S_x}{2}$. The smaller the scaling factor, the better the precision. The solutions to make the scaling factors small are either to have a smaller range $[x_{\min}, x_{\max}]$ or to use a bigger bitwidth b . In practice, for a given bitwidth, we would like to have a large range including all possible values the network can produce, but also to have small errors. These two principles are contradictory, it is the range-precision trade-off.

A.2.4 Quantized multiplication

Define $u \in [u_{\min}, u_{\max}] = [-1, 1]$ and $w \in [w_{\min}, w_{\max}] = [0, 5]$, the multiplication between two numbers from those ranges will fall into $[z_{\min}, z_{\max}] = [-5, 5]$. For 8-bit quantization, we have $S_u \approx 0.0078$, $Z_u = 128$, $S_w \approx 0.0196$, $Z_w = 0$, $S_z \approx 0.0392$, $Z_z = 128$. Given $u = -0.8$ and $w = 2.3$, we have $q_u = 25$ and $q_w = 117$. Following (25),

$$q_z = \left\lfloor \frac{S_u S_w}{S_z} (q_u q_w - q_u Z_w - q_w Z_u + Z_u Z_w) \right\rfloor + Z_z \quad (35)$$

$$= \left\lfloor \frac{0.0078 * 0.0196}{0.0392} (25 * 117 - 25 * 0 - 117 * 128 + 128 * 0) \right\rfloor + 128 \quad (36)$$

$$= 81. \quad (37)$$

The floating-point representation of q_z is $r_z = -1.8424$. r_z is close to $uv = -1.8399$. Note that we lost precision at two levels, the first time when quantizing u and v , then the second time when quantizing z , the output of the multiplication.

A.2.5 Quantized addition

As mentioned in §3.4, addition with quantized numbers can take two forms. The first form is when the two numbers to be added share the same scaling factor and zero-point. For instance, given $x_1 = -0.3$, $x_2 = 0.7$ from $[-1, 1]$, and $S_x = 0.0078$, $Z_x = 128$, we have $q_{x_1} = 90$ and $q_{x_2} = 218$. The result value y will fall into the range $[-2, 2]$, therefore $S_y \approx 0.0157$ and $Z_y = 128$. Then, because they share the same quantization parameters, following (26),

$$q_y = \left\lfloor \frac{1}{S_y} (S_x(q_{x_1} - Z_x) + S_x(q_{x_2} - Z_x)) \right\rfloor + Z_y \quad (38)$$

$$= \left\lfloor \frac{S_x}{S_y} (q_{x_1} + q_{x_2} - 2Z_x) \right\rfloor + Z_y \quad (39)$$

$$= \left\lfloor \frac{0.0078}{0.0157} (90 + 218 - 256) \right\rfloor + 128 \quad (40)$$

$$= 154. \quad (41)$$

We have $r_y = 0.4082$, while $x_1 + x_2 = 0.3999$. The second form is when the two numbers do not share the same scaling factor and zero-point. Define $a \in [a_{\min}, a_{\max}] = [-1, 1]$ and $b \in [b_{\min}, b_{\max}] = [0, 5]$, the addition between two numbers from those ranges will fall into $[c_{\min}, c_{\max}] = [-1, 6]$. We get $S_a \approx 0.0078$, $Z_a = 128$, $S_b \approx 0.0196$, $Z_b = 0$, $S_c \approx 0.0274$, $Z_c = 36$. For $a = -0.9$, $b = 3.9$, we have $q_a = 13$ and $q_b = 199$. The quantized addition result q_c , following (27), is,

$$q_c = \left\lfloor \frac{S_a}{S_c}(q_a - Z_a) + \frac{S_b}{S_c}(q_b - Z_b) \right\rfloor + Z_c \quad (42)$$

$$= \left\lfloor \frac{0.0078}{0.0274}(13 - 128) + \frac{0.0196}{0.0274}199 \right\rfloor + 36 \quad (43)$$

$$= 146 \quad (44)$$

and $r_y = 3.0140$ while $a + b = 3.0$.

A.2.6 Inference based on integer-only arithmetic

For the inference to be integer-only arithmetic, all values have to be expressed as integers. However, in the expressions described throughout the previous sections, there often are some terms involving scaling factors that are not integers (e.g. $\frac{S_u S_w}{S_z}$ in (35)). Therefore the question one might ask is how to go around this fact? Such constants are expressed as fixed-point integers, which are computed off-line (after training but before inference). The Q-format is a way to describe the properties of a fixed-point integer number. We will base the following explanations on several assumptions to simplify the concepts, as fixed-point integer arithmetic is a vast concept. A fixed-point integer having format Qi.f is said to have one sign bit, i integral bits and f fractional bits, bitwidth $1 + i + f$, a resolution of 2^{-f} and span the range $[-2^{-f}, 2^i - 2^{-f}]$. For instance, Q3.4 represents numbers in $[-8, 7.9375]$ with resolution 0.0625 and Q0.30 represents numbers in $[-1, 0.99999]$ with $\approx 9 \times 10^{-10}$. Assuming we do not have to worry about overflows, quantizing a floating-point number M to a fixed-point integer M_{fx} is given by,

$$M_{fx} = \lfloor 2^f M \rfloor. \quad (45)$$

Going from a fixed-point integer M_{fx} to floating-point number M is given by,

$$M = 2^{-f} M_{fx} \quad (46)$$

For instance, with $M = \frac{S_u S_w}{S_z} = 0.0039$ and the fixed-point representation of M in Q-format Q0.30 is $M_{fx} = 4187593$ and mapped back to floating-point as $M = 0.00389$. An equivalent expression to (46) is

$$M = M_{fx} \gg f \quad (47)$$

where \gg is the right shift operator. The last piece needed to perform integer-only inference is to incorporate the fixed-point numbers in the expressions involving floating-point constants, often of the form $q_y = \lfloor Mq \rfloor + Z_y$, which can be expressed as

$$q_y = \left\lfloor 2^{-f} M_{fx} q \right\rfloor + Z_y \quad (48)$$

$$= M_{fx} q \gg f + \quad (49)$$

$$(M_{fx} q \gg (f - 1)) \& 0x1 + Z_y. \quad (50)$$

For instance, computing (35) using the fixed-point representation of $M = \frac{S_u S_w}{S_z} = 0.0039$ in Q0.30 is given by,

$$q_z = \left\lfloor 2^{-f} M_{fx} q \right\rfloor + Z_z \quad (51)$$

$$= \left\lfloor 2^{-30}(4187593 \times -12051) \right\rfloor + 128 \quad (52)$$

$$= -\left((50464683243 \gg 30) + ((50464683243 \gg 29) \& 0x1) \right) + 128 \quad (53)$$

$$= -(46 + 1) + 128 = 81 \quad (54)$$

which is the same result obtained previously (37). We extracted the negative sign out of the binary shifts, as shifting on negative number has different behavior depending on the software and hardware implementation. Note that in practice, when we know a constant can only be positive, it will be expressed as an unsigned fixed-point integer and therefore the sign bit can be allocated to either the integral or fractional part.

Experiment	Params	Full-precision	iRNN	+PWL	Total GPU hours
LM PTB	4M	1h	13h	10h	24h
LM WikiText2	44M	37h	87h	50h	174h
ASR LibriSpeech	174M	144h	36h	12h	192h

Table 4: Details about the models parameters and training time for each different experiments setup: language modeling on PTB (LM PTB), language modeling on WikiText2 (LM WikiText2), automatic speech recognition on LibriSpeech (ASR LibriSpeech). Parameters are given in the order of millions. We report the total number of V100 GPU hours as well as the GPU hours used for each different training phase, i) pre-trained model (Full-precision), ii) quantized model without PWL (iRNN), iii) quantized model with PWL (+PWL).

A.3 Experimental details

We provide a detailed explanation of our experimental setups. The models’ number of parameters and training time are reported in Table 4.

A.3.1 LayerNorm LSTM on PTB

We provide detailed information about how the language modeling on PTB experiments are performed. The vocabulary size is 10k, and we follow dataset preprocessing as done in Mikolov et al. (2012). We report the best *perplexity* per word on the validation set and test set for a language model of embedding size 200 with one LayerNormLSTM cell of state size 200. The lower the perplexity, the better the model performs. In these experiments, we are focusing on the relative increase of perplexity between the full-precision models and their 8-bit quantized counterpart. We did not aim to reproduce state-of-the-art performance on PTB and went with a naive set of hyper-parameters. The full-precision network is trained on for 100 epochs with batch size 20 and BPTT (Werbos, 1990) window size of 35. We used the SGD optimizer with weight decay of 10^{-5} and learning rate 20, which is divided by 4 when the loss plateaus for more than 2 epochs without a relative decrease of 10^{-4} in perplexity. We use gradient clipping of 0.25. We initialize the quantized models from the best full-precision checkpoint and train from another 100 epochs. For the first 5 epochs we do not enable quantization to gather range statistics to compute the quantization parameters.

A.3.2 Mogrifier LSTM on WikiText2

We describe the experimental setup for Mogrifier LSTM on WikiText2. Note that we follow the setup of Melis et al. (2020) where they do not use dynamic evaluation (Krause et al., 2018) nor Monte Carlo dropout (Gal and Ghahramani, 2016). The vocabulary size is 33279. We use a 2 layer Mogrifier LSTM with embedding dimension 272, state dimension 1366, and capped input gates. We use 6 modulation rounds per Mogrifier layer with low-rank dimension 48. We use 2 Mixture-of-Softmax layers (Yang et al., 2018). The input and output embedding are tied. We use a batch size of 64 and a BPTT window size of 70. We train the full-precision Mogrifier LSTM for 340 epochs, after which we enable Stochastic Weight Averaging (SWA) (Izmailov et al., 2018) for 70 epochs. For the optimizer we used Adam (Kingma and Ba, 2014) with a learning rate of $\approx 3 \times 10^{-3}$, $\beta_1 = 0$, $\beta_2 = 0.999$ and weight decay $\approx 1.8 \times 10^{-4}$. We clip gradients’ norm to 10. We use the same hyper-parameters for the quantized models from which we initialize with a pre-trained full-precision and continue to train for 200 epochs. During the first 2 epochs, we do not perform QAT, but we gather min and max statistics in the network to have a correct starting estimate of the quantization parameters. After that, we enable 8-bit QAT on every component of the Mogrifier LSTM: weights, matrix multiplications, element-wise operations, activations. Then we replace activation functions in the model with quantization-aware PWLs and continue training for 100 epochs.

We perform thorough ablation on our method to study the effect of each component. Quantizing the weights or the weights and matrix multiplications covers about 0.1 of the perplexity increase. There is a clear performance drop after adding quantization of element-wise operations with an increase in perplexity of about 0.3. This is both due to the presence of element-wise operations in the cell and hidden states computations (2, 3) affecting the flow of information across timesteps and to the residual connections across layers. On top of that, adding quantization of the activation does not impact the performance of the network.

A.3.3 ESPRESSO LSTM on LibriSpeech

The encoder is composed of 4 CNN-BatchNorm-ReLU blocks followed by 4 BiLSTM layers with 1024 units. The decoder consists of 3 LSTM layers of units 1024 with Bahdanau attention on the encoder’s hidden states and residual connections between each layer. The dataset preprocessing is exactly the same as in Wang et al. (2019b). We train

LSTM	ms	iter/s	speedup
Full-precision	130	7.6	1.00×
iRNN w/ PWL32	84	11.8	1.54×
iRNN w/ PWL8	61	14.9	1.95 ×
iRNN w/o QAct	127	7.8	1.02×

Table 5: Inference measurements on an anonymous smartphone based on a custom fork from PyTorch 1.7.1. The model is a one LSTM cell with a state size of 400. Milliseconds (ms) and iterations per second (iter/s) are averaged across 100 runs.

iRNN Mogrifier LSTM	val	test
w/o PWL	60.40 ± 0.05	57.90 ± 0.01
w/o Quantized Activations	60.40 ± 0.03	57.95 ± 0.003
w/o Quantized Element-wise ops	60.08 ± 0.10	57.61 ± 0.23
w/o Quantized Matmul	60.10 ± 0.05	57.64 ± 0.10
w/o Quantized Weights (Full-precision)	60.27 ± 0.34	58.02 ± 0.34

Table 6: Ablation study on quantized Mogrifier LSTM training on WikiText2. iRNN w/o PWL is the quantized model using LUT instead of PWL to compute the activation function. Best results are averaged across 3 runs, and standard deviations are reported.

the model for 30 epochs on one V100 GPU, which takes approximately 6 days to complete. We use a batch size of 24 while limiting the maximum number of tokens in a mini-batch to 26000. Adam is used with a starting learning rate of 0.001, which is divided by 2 when the validation set metric plateaus without a relative decrease of 10^{-4} in performance. Cross-entropy with uniform label smoothing $\alpha = 0.1$ (Szegedy et al., 2016) is used as a loss function. At evaluation time, the model predictions are weighted using a pre-trained full-precision 4-layer LSTM language model (shallow fusion). Note that we consider this language model an external component to the ESPRESSO LSTM; we do not quantize it due to the lack of resources. However, we already show in our language modeling experiments that quantized language models retain their performance. We refer the reader to Wang et al. (2019b) and training script⁴ for a complete description of the experimental setup. We initialize the quantized model from the pre-trained full-precision ESPRESSO LSTM. We train the quantized model for only 4 epochs due to the lack of resources. The quantized model is trained on 6 V100 GPUs where each epoch takes 2 days, so a total of 48 GPU days. The batch size is set to 8 mini-batch per GPU with maximum 8600 tokens. We made these changes because otherwise, the GPU would run out of VRAM due to the added fake quantization operations. For the first half of the first epoch, we gather statistics for quantization parameters then we enable QAT. The activation functions are swapped with quantization-aware PWL in the last epoch.

A.4 Inference measurements

We implemented an 8-bit quantized integer-only LSTM with PWL model based on a custom PyTorch (Paszke et al., 2019) fork from 1.7.1. We implemented an integer-only PWL kernel using NEON intrinsics. We benchmark the models on an anonymous smartphone using the `speed_benchmark_torch` tool⁵. We warm up each model for 5 runs and then measure the inference time a hundred times and report an average. The sequence length used is 128, and the batch size is one. We benchmark our iRNN LSTM model using PWLs with 32 pieces, and 8 pieces which achieve up to $2\times$ speedup. We also evaluate our iRNN with full-precision computations (iRNN w/o QAct) for the activation where no speedup was observed for this state size. We believe it is due to round-trip conversions between floating-points and integers (Table 5). There is a lot of room for improvements to achieve even greater speedup, such as writing a C++ integer-only LSTM cell, fusing operations, and better PWL kernel implementation.

⁴https://github.com/freewym/espresso/blob/master/examples/asr_librispeech/run.sh

⁵https://github.com/pytorch/pytorch/blob/1.7/binaries/speed_benchmark_torch.cc

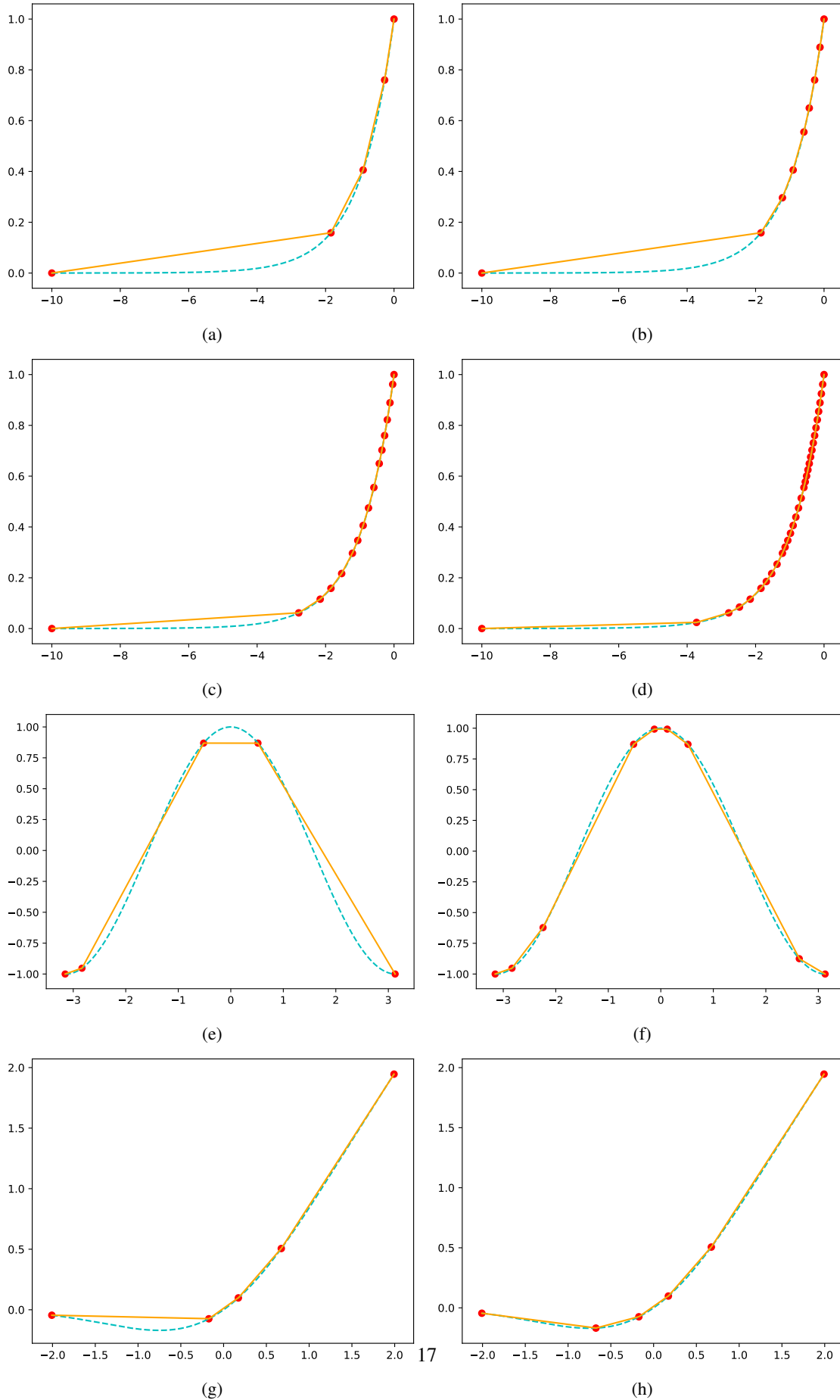


Figure 3: Quantization-aware PWL for several functions: exponential function approximation over $x \in [-10, 0]$ with a) 4, b) 8, c) 16, d) 32 pieces; cosine over $x \in [-\pi, \pi]$ with e) 4, f) 8 pieces; GaU (Handryks and Gimpel, 2016) over

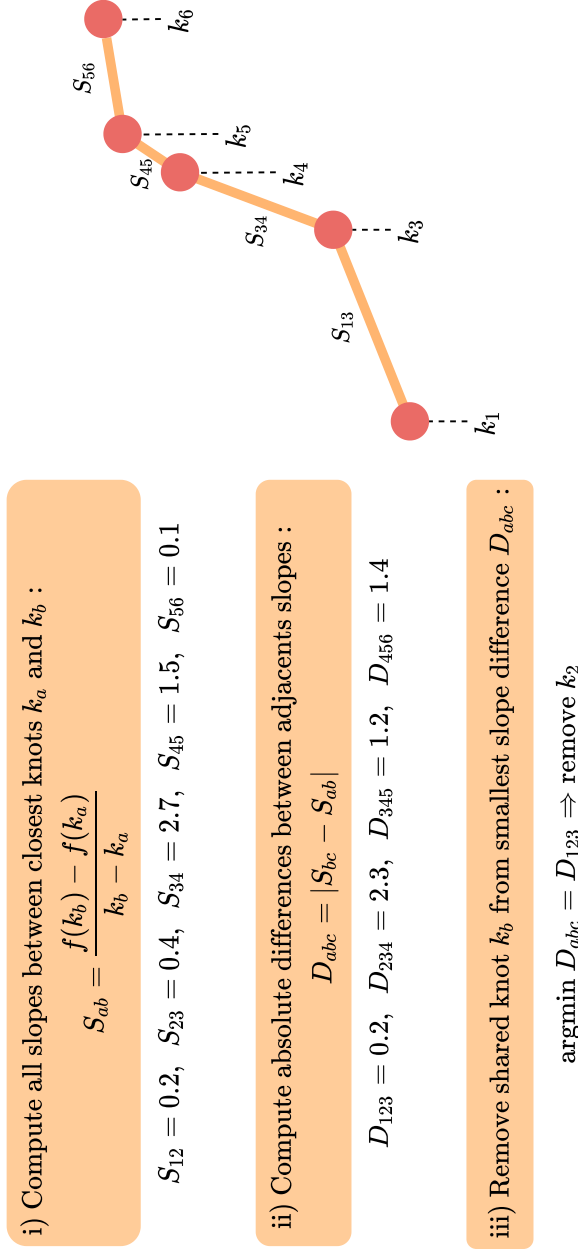


Figure 4: Example of an iteration from our proposed quantization-aware PWL Algorithm 1. The algorithm proceeds to reduce the number of pieces by merging two similar adjacent pieces. In this figure, the slopes S_{12} and S_{23} are the most similar pieces; therefore, the knot k_2 is removed.

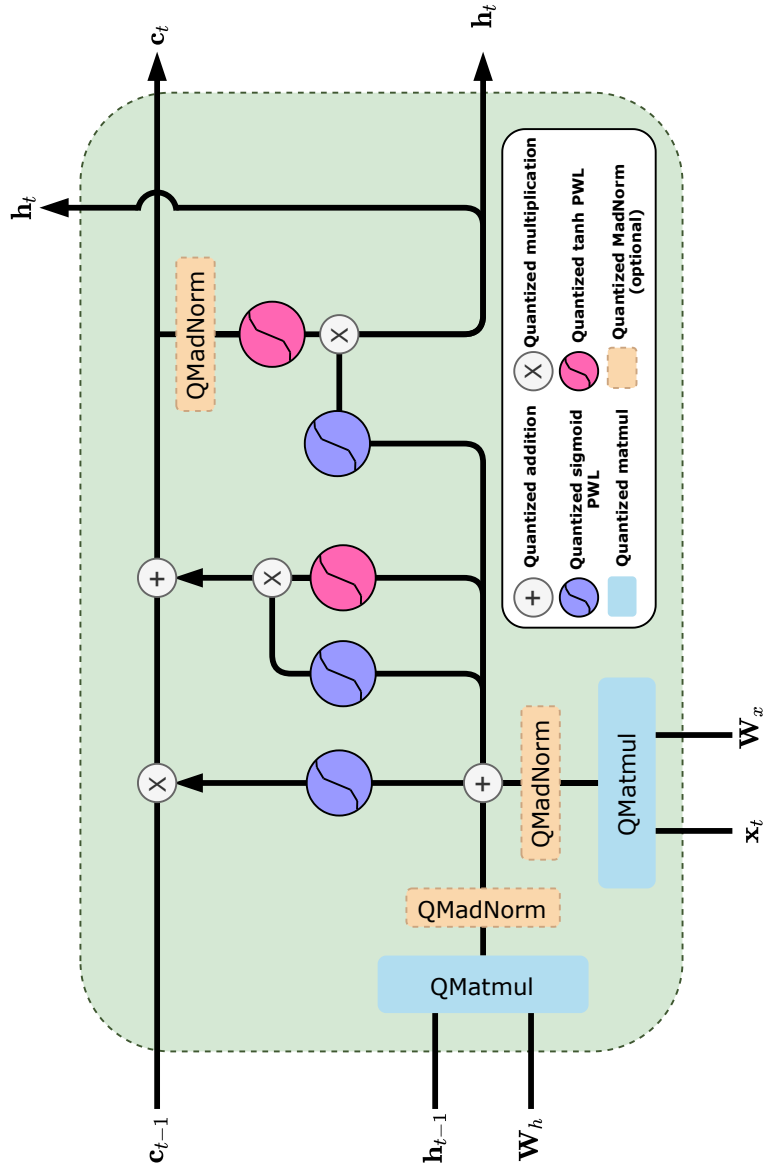


Figure 5: Example of an integer-only LSTM cell (iLSTM). Layer normalization change to quantized integer friendly MadNorm (QMadNorm), full-precision matrix multiplications change to integer matrix multiplication (QMatmul), sigmoid and tanh activations are replaced with their corresponding piecewise linear (PWL) approximations.

Full-precision model	val	test
LayerNorm LSTM	98.58 \pm 0.35	94.84 \pm 0.21
MadNorm LSTM	97.20 \pm 0.47	93.63 \pm 0.74

Table 7: Word-level perplexities on PTB for a full-precision LSTM with LayerNorm and a full-precision model with MadNorm. Best results are averaged across 3 runs, and standard deviations are reported.

Algorithm 1: The algorithm recursively reduced the number of pieces until the wanted number of pieces is achieved. The algorithm needs to be provided the function to approximate f , the input scaling factor S_x and zero-point Z_x , the quantization bandwidth b and the number of linear pieces wanted. One iteration of `select_knots` can be viewed in Figure 4.

```

def select_knots (knots, intercepts, pwl_nb) :
    dknots  $\leftarrow$  knots[1:] - knots[:-1]
    dintercepts  $\leftarrow$  intercepts[1:] - intercepts[:-1]
    slopes  $\leftarrow$  dintercepts/dknots
    if len (slopes) == pwl_nb:
        return knots, slopes, intercepts
    else:
        diff_adj_slopes  $\leftarrow$  |slopes[:-1] - slopes[1:]|
        knot_index_to_remove  $\leftarrow$  argmin diff_adj_slopes
        remaining_knots  $\leftarrow$  knots.remove(knot_index_to_remove)
        remaining_intercepts  $\leftarrow$  intercepts.remove(knot_index_to_remove)
        return select_knots (remaining_knots, remaining_intercepts, pwl_nb)

def create_quantization_aware_pwl (f, input_scale, input_zero_point, b, pwl_nb) :
    quantized_knots  $\leftarrow$  [0, ..., 2b - 1] // Generate every  $q_x$ 
    knots  $\leftarrow$  input_scale  $\odot$  (quantized_knots - input_zero_point) // Generate every  $r_x$ 
    intercepts  $\leftarrow$  f(knots)
    {knots, slopes, intercepts}  $\leftarrow$  select_knots (knots, intercepts, pwl_nb)
    return knots, slopes, intercepts

```
